Performance Evaluation of UV Reactor Using Optical Diagnostic Techniques

Siamak Elyasi and Fariborz Taghipour
Chemical and Biological Engineering Dept., University of British Columbia, Vancouver, BC, Canada V6T 1Z3

DOI 10.1002/aic.12251
Published online April 16, 2010 in Wiley Online Library (wileyonlinelibrary.com).

Conventionally, the performance of a UV reactor is evaluated using the concentration of photoreactive chemicals at the outlet vs. the inlet. This research presents a novel method for measuring the concentration distribution of a photoreactive chemical inside a photoreactor using a modified planar laser-induced fluorescence method. The fluence distribution was measured for a pilot scale photoreactor under different operating conditions. The visualized result of the fluence distribution revealed significant information about the local/overall performance of the photoreactor. This method is a powerful diagnostic tool for the determination of the local performance inside a UV reactor, as well as for the evaluation of models simulating UV reactor behavior.
 AIChE J, 57: 208–217, 2011
Keywords: PLIF, UV reactor, performance evaluation

Introduction

In 1955, Switzerland and Australia started using UV-disinfecting municipal drinking water stations. By 1985, the number of such stations had increased to 500 and 600, respectively, in these two countries.[1] UV-based photolysis and photo-initiated oxidation have great potential for the inactivation of microorganisms and degradation of a wide range of contaminants in water. The effect of UV on microorganisms is due to a photochemical reaction caused by the absorption of radiant energy, which results in photochemical damage to their DNA and, hence, their inactivation. UV technology is recognized as one of the best available technologies for water disinfection. Many major cities in North America including New York City, with its 6.7 m^3/s water consumption, are installing UV reactors for water treatment. The electrical power consumption of installed UV facilities are 30–180 kJ/m^3.[2] Any improvement in the performance of such a system would lead to considerable environmental and economic gains.

In addition to disinfection of microorganisms, UV can also be applied to the degradation of persistent chemical contaminants in water when used in combination with an oxidant, such as hydrogen peroxide. The mechanism for the photolysis of hydrogen peroxide is the splitting of the molecule into two hydroxyl radicals, which are highly reactive components. The redox potentials of hydroxyl radicals, after fluorine, are the highest among other oxidizers, such as atomic oxygen and chlorine dioxide.[3] This implies that hydroxyl radicals will oxidize most organic persistent contaminants.[4] UV-hydrogen peroxide can be used for treating water/wastewater that contains contamination levels of <1000 ppm[5] or chemical oxygen demand (COD) levels <5 kg/m^3.[6] The process is applicable to small- to medium-sized industrial units for the treatment of contaminated water and for the production of highly pure water for the pharmaceutical and microelectronic industries.[7]

The conventional method of evaluating the performance of a UV reactor is to compare the concentrations of pollutants or active microorganisms at the outlet of the reactor with those at the inlet.[8–12] There has been considerable effort put into improving this technique by introducing various chemicals and new methods. Bohrerova et al.[13] developed a method for calculating the received UV fluence through a photoreactor using photochemically active fluorescent microspheres. This technique was able to calculate the fluence rate distribution in the UV reactor using the concentrations at the outlet. Although this method can provide valuable information on fluence distribution inside a UV reactor, the

Correspondence concerning this article should be addressed to S. Elyasi at siamak.elyasi@gmail.com.

reactor itself is treated as a black box and the fluence distribution through the UV reactor is not revealed directly.

In this research, for the first time (to the author's knowledge), a method is presented for mapping the fluence distribution in the entire UV reactor by adapting and modifying conventional planar laser-induced fluorescence (PLIF). Rhodamine WT (RhWT), a fluorescent chemical, is resistant to photolysis, but is oxidized easily by hydroxyl radical.[14,15] If the RhWT solution is excited with a green laser at 532 nm, the irradiance of the re-emitted light at 588 nm from the solution is linearly proportional to the concentration of RhWT. This phenomenon can be used to trace UV photoreactive solutions (RhWT and hydrogen peroxide) in a UV reactor to determine the received fluence by the solution. This qualitative concentration diagnostic method is a very powerful tool for the nonintrusive visualization of the concentration and the UV fluence profile inside a UV reactor. This method can reveal the existence of problematic zones in the photoreactor at various design and operating conditions. Therefore, mapping the profile of concentration and fluence in the reactor using this method can have a significant impact on understanding the reactor behavior. This can lead to alternative UV reactor designs with improved performance. This method cannot be used directly for industrial photoreactors, considering it requires the body of the reactor to be manufactured from optically accessible (transparent) material. In addition, for reactors with relatively large diameter, a scanning method should be employed to first find the concentration close to the reactor wall and then continue the scanning up to the center of the reactor, taking into account any absorbance correction. However, this technique could be directly used for small pilot scale transparent reactors to better understand the reactor behavior. The information obtained from this method can also be used for comprehensive evaluation of models simulating the performance of UV reactors (e.g., computational fluid dynamics [CFD] models).

Principles of the measurement techniques

Planar Laser-Induced Fluorescence. Fluorescence occurs in some chemicals because photons absorbed by the chemical trigger the emission of more photons with longer wavelengths. For a clear solution (no particulates), the re-emitted radiant energy (or power) can be calculated using the quantum efficiency, Θ_s, denoting the ratio of the total energy emitted by a fluorescent chemical per quantum of absorbed energy. Combining quantum efficiency and the Beer-Lambert law, the re-emitted power is:

$$P_V(x,y,z) = \frac{2.303 T_s}{{l_{s,p}}^2}\varepsilon_{\lambda s,f} c_f \Theta_s I_0 \exp\left(-\int_0^{l_{s,p}}\left(2.303\sum_{i=1}^{n}\varepsilon_{\lambda s,i}c_i\right)dl\right), \quad (1)$$

where P_V, $l_{s,p}$, T_s, $\varepsilon_{\lambda s}$, c, I_0, n, λs, l, x, y, and z are volumetric emitted power, distance of the investigation point from the light source, portion of light that passes through the solution, molar extinction coefficient (at wavelength λs nm), concentration of all chemicals (index i stands for the ith component and f for the fluorescent chemical), the intensity of light at its source, the number of chemicals, wavelength of photons leaving the light source, length on the beam pathway, and coordinates of the studied point in the solution, respectively. The fraction of light that reaches the point in the solution (T_s) depends on the number of interfaces that the rays pass through and the characteristics of the interfaces as reflectors.

If the emission of each element in the fluorescent solution is assumed to be diffusive, the energy captured by an array of sensors (charged-coupled device [CCD] of a digital camera) or a single sensor is:

$$E_c(x_c,y_c,z_c) = \frac{T_c}{4\pi l_{c,p}^2}\Theta_c P_V t \Delta V \Delta A_{xc,yc,zc}\cos\theta_{c,p}\exp\left(\int_0^{l_{c,p}}\left(\sum_{i=1}^{n}\varepsilon_{\lambda e,i}c_i\right)dl\right), \quad (2)$$

where E_c, T_c, $\varepsilon_{\lambda e}$, $l_{c,p}$, Θ_c, t, ΔV, ΔA, $\theta_{c,p}$, x_c, y_c, and z_c are energy captured by the sensor (the value of each pixel on the CCD of camera), the fraction of the emitted light that reaches the sensor, the molar extinction coefficient (at wavelength λe nm), the distance between the sensor and emitter, the quantum efficiency of the sensor or CCD of the camera, the exposure (or integration) time of the sensor, the glowing volume element in the solution, the active area of the sensor or pixel area on the CCD of a camera, the angle between the normal vector of the sensor area and the incident ray from the emitter, and the coordinates of the sensor (pixel), respectively.

Due to the terms involving the absorbance of photons by the medium, Eq. 2 shows high nonlinearity between the concentration of fluorescent chemical in the solution and the recorded value on the pixels of the CCD of a camera. Equation 2 can be simplified if the following criteria are respected:

(1) Chemical concentrations are relatively low, in which case, the absorption of photons (from the source and re-emitted from the fluorescent chemical) can be ignored.

(2) The position of the laser source, the studied solution, and the camera are fixed during the experiment. As a result, all constants can be integrated into one factor as a setup coefficient.

(3) The integration time of the camera is longer than the lifetime of the fluorescent chemical for a pulse laser source.

As a result, the simplified equation for each point in the solution and corresponding point on the CCD of a digital camera is:

$$E_c(x_c,y_c,z_c) = K_{setup}(x_c,y_c,z_c)I_0 c_f(x,y,z) + K_{offset}(x_c,y_c,z_c), \quad (3)$$

where K_{setup} are K_{offset} are the setup and offset coefficients (slope and intercept) for each pixel on the CCD of a camera. Omitting the offset term, an equation is derived similar to the one presented by Karasso and Mungal.[16]

The setup coefficient (K_{setup}) takes all geometrical, optical and operational parameters into consideration. The offset coefficient (K_{offset}) is the produced analog current by the CCD of a digital camera when I_0 is equal to zero (dark current), in order to account for any background optical noise. The term I_0 should not be omitted because the beam emerging from the laser is nonuniform due to heterogeneities in the lasing medium.

Chemical kinetics

Hydroxyl radicals have great potential for decomposing a wide range of organic and inorganic contaminants in water.[4] The hydroxyl radicals can be produced from oxidant chemicals, such as ozone, hydrogen peroxide, and oxygen in the presence of UV radiation, e.g.,

$$H_2O_2 + \boldsymbol{hv} \longrightarrow 2OH^{\circ} \quad (4)$$

Hydroxyl radical oxidation, direct oxidation, and photolysis are the three primary reactions that take place during the degradation of organic materials in a UV-hydrogen peroxide system[17]:

$$\text{Direct oxidation : RH (organics)} + H_2O_2 \longrightarrow \text{Oxidized product} + H_2O, \quad (5)$$

$$\text{Photolysis : RH (aq)} + hv \longrightarrow RH^{*} \longrightarrow \text{Product}, \quad (6)$$

$$\text{Hydroxyl radical oxidation : RH} + OH^{\circ} \longrightarrow \text{Intermediates} \longrightarrow \text{Product}. \quad (7)$$

The rate of reaction of an organic material (in this case, the fluorescent chemical) is the algebraic summation of all three of these reactions. The limiting reaction is often the production of the hydroxyl radicals, which is a linear function of the UV radiation distribution in the photoreactor. Other radicals, intermediates, and byproducts are formed and can potentially react with the organic materials (RH) that is not shown in Reaction 7. The proposed reaction set is a generalized form of an UV advanced oxidation process initiated with hydroxyl radical. To avoid dealing with complicated mechanisms for reaction kinetics, it is a common practice to derive the general rate of reactant conversion for direct oxidation, photolysis, and hydroxyl radical oxidation. This approach has been taken here, while it is acknowledged that the proposed reaction rates are the overall rate of chemical degradation, rather than the true rate for individual reactions. A more comprehensive reaction mechanism has been proposed by Tsai and colleagues.[18]

Experimental

Materials and chemicals

The fluorescent chemical was RhWT, abbreviated as RhWT, with Chemical Abstracts Service Registry number 37299-86-8 and the index name xanthylium, 9-(2,4-dicarboxyphenyl)-3,6-bis(diethlamino)-, chloride, disodium salt in a 20 wt % aqueous solution. RhWT is a bright fluorescent red dye originally developed for water tracing applications. Potassium iodide, potassium iodate, and borax were used to calibrate the UV radiant energy passing through the bench-scale photoreactor. Hydrogen peroxide was selected as an oxidant and was measured using potassium iodide, sodium hydroxide, and ammonium molybdate tetrahydrate. All chemicals were obtained from Fisher Scientific, excluding RhWT and ammonium molybdate tetrahydrate, obtained from Turner Designs and Acros Organics, respectively.

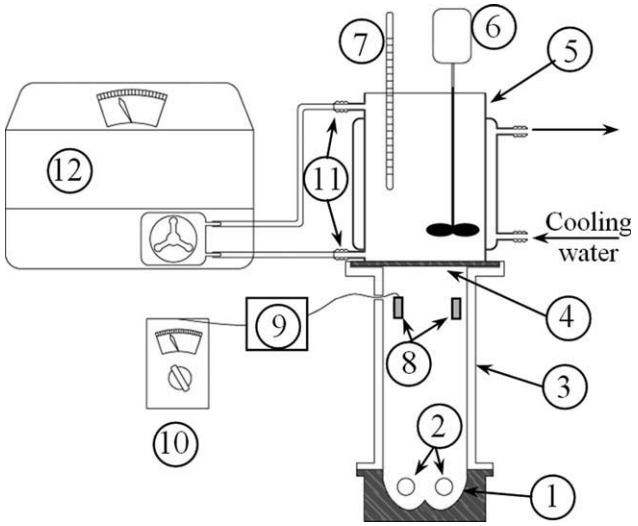

Figure 1. Collimated-beam photoreactor setup consisting of polished aluminum reflector (1), mid-size UV lamps (2), collimator (3), quartz window (4), jacketed reactor body (5), variable speed stirrer (6), thermometer (7), UV sensors (8), amplifier (9), voltmeter (10), sampling ports (11), and UV spectrophotometer with circulating pump (12).

Reaction rate measurement under controlled conditions in collimated-beam photoreactor

The chemical and photochemical reactions of RhWT and hydrogen peroxide were measured using a customized collimated beam photoreactor. The photoreactor (Figure 1) was comprised of two mid-size UV lamps, a UV radiation reflector, a UV beam collimator, a double-jacketed reactor with a volume of 250×10^{-6} m^3 and a round quartz (0.003 m thickness) at the bottom, a variable speed stirrer at the top of the reactor, and two UV sensors (SIC01M-C from Roithner LaserTechnik) below the quartz window connected to an amplifier (Multifunctional 2-Channel Amplifier Board from Roithner LaserTechnik). The emission spectrum of the UV lamp provided by the supplier, Emperor Aquatics is shown in Figure 2. The voltage signal from the amplifier was recorded using a multimeter (MultiPro 530 from Extech Instruments) and a computer. The photoreactor sample port (bottom) was connected to a flow-through cuvette of a UV-Vis spectrometer (Cary 100) via its circulating pump. The sampling solution was returned to the reactor via the top sampling port. This configuration allowed online measurement of the optical density at different wavelengths during the reaction. Figure 1 shows the configuration of the setup.

The concentration of RhWT was measured using its absorbance at 555.5 nm by the UV-Vis spectrophotometer. To investigate the effect of hydrogen peroxide on the absorbance of RhWT, different solutions of hydrogen peroxide and RhWT at various concentrations were tested. The concentration of hydrogen peroxide was measured using the method presented by Klassen et al.[19] Hydrogen peroxide can oxidize an iodide solution in alkaline pH to generate I_3^- ions. The absorbance at 352 nm reveals the concentration of this ion

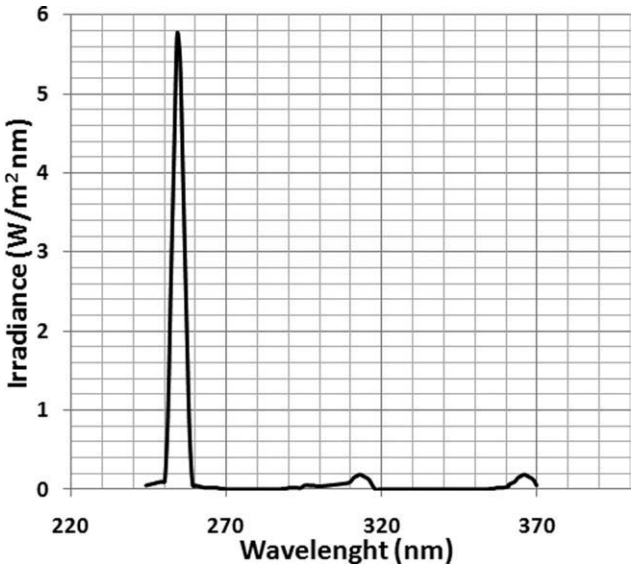

Figure 2. UV lamp emission spectrum.

using an UV-Vis spectrometer considering the molar extinction coefficient of the ion.

UV radiant energy that passed through the photoreactor was measured using the iodide–iodate actinometer method presented by Rahn et al.[20] The iodide/iodate solution was fed into the photoreactor after the UV lamp has been turned on and stabilized for 30 min. The online UV-Vis spectrophotometer was used to continuously measure the absorbance of the solution at 352 nm, which is related to the concentration of I_3^- or absorbed UV radiant energy in the reactor. At the same time, the signals (voltage) produced by the UV sensors below the quartz window were recorded as reference points for the period of measurement. The absorbance (concentration) results yielded the amount of radiant energy entering into the photoreactor, considering the quantum yield of the iodide–iodate actinometer.

The direct oxidation rate of RhWT was measured by mixing a solution of RhWT and hydrogen peroxide with concentrations of 791 $\pm$ 4 ppb and 9.72 $\pm$ 0.08 ppm, respectively, in the collimated-beam photoreactor for a 2-h period, while the UV lamp was not operating.

The photolysis rate of RhWT was evaluated in the photoreactor while the UV lamp was operating in a stabilized mode (as indicated by a constant voltage signal from the sensors). The photoreactor was charged with RhWT solutions (800–100 ppb), and during the process of photolysis, their concentrations were measured for a period of 2 h. As the rate of photolysis is a direct function of the reactant concentration, a relatively high range of RhWT concentration was applied to enhance the photolysis rate and to better determine the existence of any potential direct photolysis reaction.

The photo-initiated oxidation rate of RhWT with hydrogen peroxide and UV radiation was determined using RhWT solutions with a concentration of 126 $\pm$ 1 ppb and hydrogen peroxide with a concentration of 10.14 $\pm$ 0.05 ppm in the collimated-beam photoreactor. The concentration of RhWT was measured as a function of time using the online spectrophotometer, and the concentration of hydrogen peroxide at the end of reaction (9.77 $\pm$ 0.05 ppm) was determined using the I_3^- method. In this way, the overall rate of RhWT degradation, including all the reactions between different radicals and reactive byproducts with RhWT are measured. In the other word, the concentration of RhWT as function of received UV dose results in an empirical overall reaction rate applicable to specific concentrations of RhWT and hydrogen peroxide under study.

The selected concentrations are based on: (1) UV transmittance of the medium that is important for photo-initiated oxidation of RhWT (higher concentrations of hydrogen peroxide and RhWT decrease the UV transmittance of the medium dramatically), (2) absorption of the laser light, considering fluorescent effect of RhWT (higher concentrations suppresses the absorption), (3) concentration gradient of RhWT in the pilot scale photoreactor (lower RhWT concentrations cause higher gradient and higher error consequently). The values were adjusted after several trials and errors, based on the measurements of absorption at 254, 532, 555.5, and 588 nm, as well as determining the reaction rates in the collimated beam and pilot scale reactor using different concentrations.

Concentration measurements by PLIF in flow-through photoreactor

Flow-Through Photoreactor. A flow-through UV photoreactor was used to map the fluence distribution using modified PLIF. Considering the PLIF criteria,[21] the flow-through UV photoreactor was carefully designed to increase the accuracy of the measurements by minimizing or eliminating possible optical noise. The height and width of the photoreactor were minimized to reduce optical absorbance. The reactor body was built of glass to be UV resistant and to eliminate the staining effect of RhWT on the reactor surface. A high-performance, high-output, low-pressure UV lamp (200 W, arc length 1.07 m from Emperor Aquatics) installed inside a quartz tube below the reactor was used as the radiation source. The emission spectrum of this lamp is similar to the one shown in Figure 2 with higher irradiance/fluence rate. The UV reactor configuration and its dimensions are provided in Figure 3. A schematic diagram of the entire PLIF experimental system consisting of the pump, piping, instrumentation, and storage tanks, is shown in Figure 4.

The UV lamp was operated for 30–45 min to allow stabilization. During this period, the pump circulated distilled water at 20 $\pm$ 1°C from tank 1 through the photoreactor. The photoreactive solution, hydrogen peroxide (10.30 $\pm$ 0.05 ppm) and RhWT (126 ppb) at 21.4 $\pm$ 0.3°C, was filled into tank 2. Once the UV lamp stabilized, distilled water was pumped out to the drain system and the photoreactive solution was fed into the reactor. Flow rate and temperature were recorded using a calibrated flow/temperature meter (FluidVision 4000 from Proteus Industries). The concentration of RhWT (at the outlet of the photoreactor) was measured by an online spectrophotometer. The temperature of the solution was kept at 20 $\pm$ 1°C, and cooling air was passed through the sleeve of the photoreactor at 1.33 $\pm$ 0.16 $\times 10^{-3}$ m^3/s. This procedure guaranteed isothermal photoreaction in the reactor. Returned liquid was collected into tank 1 for final treatment, the deterioration of the RhWT, before sending it to the drain.

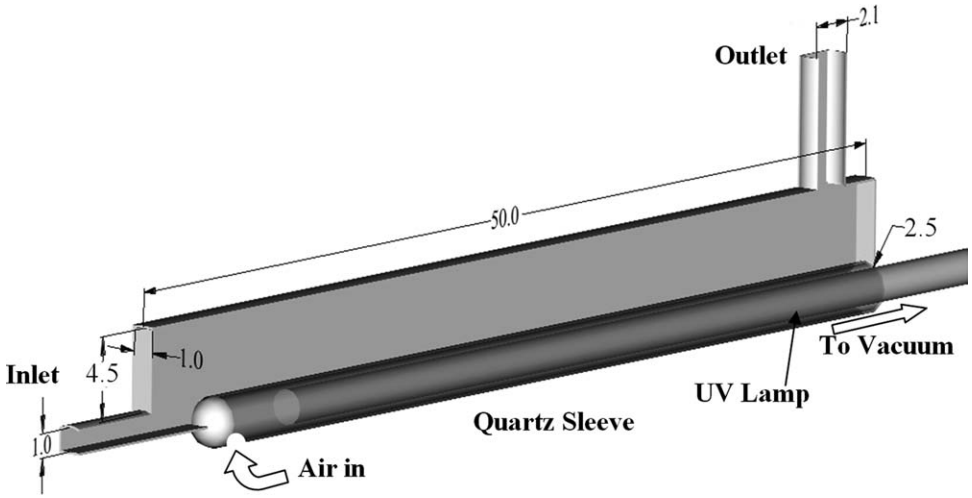

Figure 3. The flow-through UV photoreactor used for PLIF measurements (all dimensions are expressed in cm).

PLIF tests

PLIF Setup. A conventional PLIF system consist of a single camera, a laser source, a synchronizer unit, and an image acquisition/processing system. Typically, a pulse laser having a uniform beam energy is used. For a fixed laser energy (e.g., 10×10^{-3} J), a pulse-to-pulse laser beam energy variation of about $\pm 7\%$ has been reported by Melton and Lipp.[21] In our experiments, similar energy variations were measured. Measuring the energy value of the laser beam (I_0 in Eq. 3) improves the accuracy for calculating the local concentration of the fluorescent species. For this research, a second camera was integrated into the conventional system to achieve a local laser energy content measurement by mapping the laser energy at each pulse. The beam from the laser source at 532 nm (Nd:YAG laser, Solo III from NewWave Research) was divided in two using a beam splitter. One part of the beam acted as a light sheet after passing through the reactive solution in the photoreactor, and this caused the light to be re-emitted at 588 nm. The re-emitted light was captured using a 12-bit digital camera (C8484 from Hamamatsu) equipped with a high-pass filter (>550 nm). The other part of the beam was reflected from a barium sulfate-coated glass for measuring the spatial laser energy at each pulse and captured by a second camera with a band-pass filter (532 ± 10 nm). Synchronization, image acquisition, and image processing were performed by a FlowMap system hub from Dantec Dynamics. Figure 5 shows the configuration of the PLIF setup.

Calibration Procedure. During the calibration and measurement, the coordinates of the cameras, laser source, and reactor were unchanged, and the temperature of the solutions remained at 20 ± 1°C. Hydrogen peroxide solutions (9.7 ± 0.6 ppm) with different RhWT concentrations (10–130 ppb) were passed through the reactor, and 400 images were captured for each concentration using both cameras while the laser operated. The value of each pixel on the captured images (E_c in Eq. 3) at each location (x_c, y_c, z_c) was subtracted from the value of each pixel at the same location while the laser was not operating (to correct for any background light) and

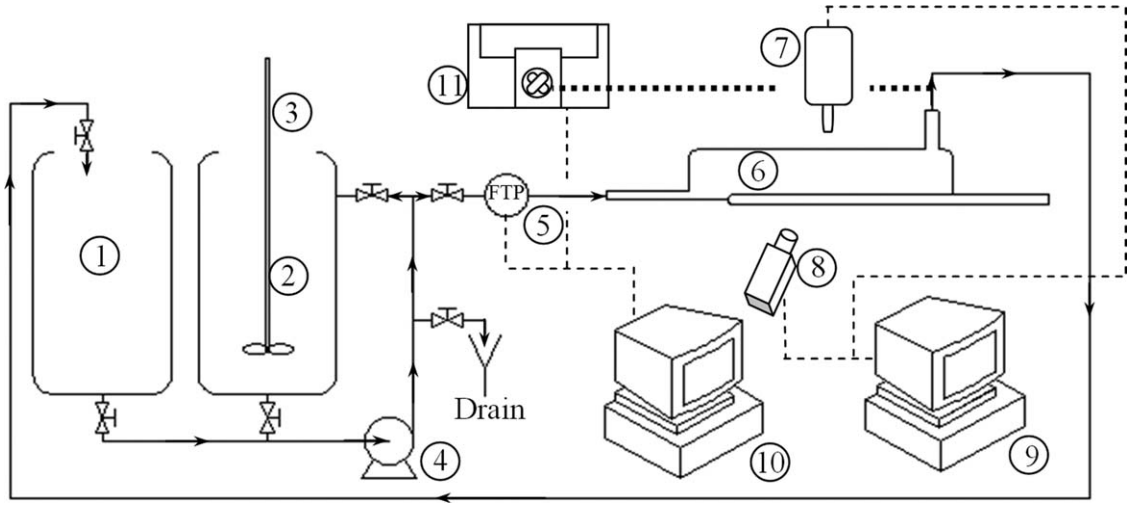

Figure 4. Schematic of pilot-scale photoreactor consisting of: product reservoir (1), feed reservoir (2), stirrer (3), centrifugal pump (4), flow/pressure/temperature meter (5), photoreactor (6), laser source (7), digital camera (8), PLIF control unit (9), data acquisition system (10), and online spectrophotometer (11).

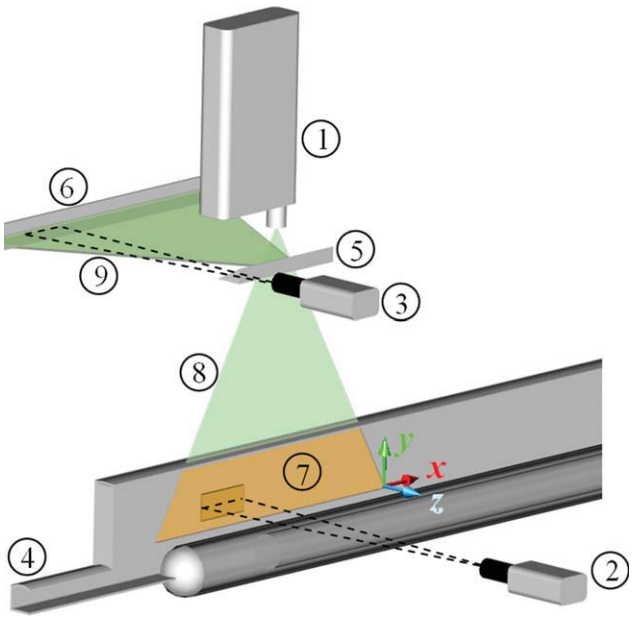

Figure 5. Schematic view of the PLIF apparatus for measuring concentrations of the photoreactive solution.

The setup consists of: a pulsed laser at 532 nm (1); a digital camera with a high-pass filter (2), a digital camera with a band-pass filter (3), a photoreactor (4), a beam splitter (5), a diffusive reflector (6), re-emitted light at 588 nm (7), and laser sheets (8, 9). [Color figure can be viewed in the online issue, which is available at wileyonlinelibrary.com.]

normalized by dividing by the total value of the total reflected light (I_0) captured by the second camera (to correct for any variation in the pulsed bean energy). Finally, the average of 400 normalized images for different concentrations of RhWT were used to calculate K_{setup} and K_{offset}, the slope and intercept, for each pixel on the image. For each pixel on the image, the corresponding K_{setup} and K_{offset} were calculated separately and saved on an array with the same size as that of the image. As a result, each pixel has its own linear function of RhWT concentration vs. emitted light (calibration line), unlike the conventional PLIF method that one curve interprets the concentration (vs. emitted light) for the entire pixels on the image. The results of the calibration calculation were two-dimensional arrays of K_{setup} and K_{offset} for each pixel in the reactor excited by the laser sheet. Knowing the emitted light for each pixel (captured by the camera), the unknown concentration for that pixel on the image (and therefore the point in the solution) was calculated using the pixel K_{setup} and K_{offset} (to correct for both the background light and any inconsistency in the pulsed bean energy).

The presence of hydrogen peroxide in the calibration procedure is necessary to achieve accurate results, as the fluorescent characteristic of RhWT heavily depends on the oxidant content of the solution.[22] Because the photoreactive solution is bleached with a high-power laser pulse, the solution should flow through the reactor and be replaced with fresh solution for each run.

Rhodamine WT has a fluorescent effect under UV radiation (254 nm), which creates a background (optical noise) in the final measurement. To quantify and make corrections for this background noise, the UV reactor ran (with the UV lamp on) with different concentrations of RhWT without hydrogen peroxide, and 400 images were captured in the absence of the laser pulse. The average values of the images were used to calculate the glowing background image (offset) for the final concentrations in the UV reactor.

To reconstruct the concentration profile throughout the entire reactor, the length of the reactor was divided into three zones: the inlet, the middle, and the outlet zones. Based on the length of the reactor and the field of view of the camera, adequate overlap was considered between two adjacent zones.

Concentration Measurement. A stock solution of hydrogen peroxide (10.30 $\pm$ 0.05 ppm) and RhWT (126 ppb) at 21.4 $\pm$ 0.3°C was fed into the reactor once the UV lamp was stabilized. Three different mass flow rates (0.006 $\pm$ 0.002, 0.015 $\pm$ 0.002, and 0.020 $\pm$ 0.002 kg/s, which correspond to mean axial velocities of 0.06 $\pm$ 0.02, 0.15 $\pm$ 0.02, 0.20 $\pm$ 0.02 m/s, respectively, at the inlet of UV photoreactor) were tested. For each operating condition, the inlet, the middle, and the outlet zones of the reactor were studied, and 400 images were captured for each section. The average of the energy captured (value) in the images after subtracting the glowing effect of the background (offset) was used for the concentration calculation. This procedure was applied to all three zones covering the entire length of the reactor.

To evaluate the effect of intermediate compounds and byproducts on the absorbance of the RhWT solution and impacting the UV-Vis spectrophotometer results, fresh RhWT in hydrogen peroxide and RhWT reacted solutions were examined. Samples of fresh RhWT (different concentrations) in hydrogen peroxide (10 $\pm$ 1 ppm) solution and irradiated (at different UV doses) RhWT (131 $\pm$ 11 ppb) in hydrogen peroxide (10 $\pm$ 1 ppm) solution were prepared. The re-emitted light from the solution (using a continues 5 mw green laser at 532 nm for sample excitation, and 1 cm pathway cuvette as sample holder) after passing through a high-pass filter (>550 nm) was captured using photodiode (PIN-10D from UDT Sensors, with 100 mm^2 active area) in a dark room. The signals from photodiode were amplified by 10 (using SC-2040 Simultaneously Sampling Differential Amplifier, from National Instrument) and the output voltages were measured using a voltmeter. For each sample, the absorbance at 555.5 nm was simultaneously measured using a spectrophotometer. Figure 6 shows the absorbance at 555.5 nm vs. re-emitted light (voltage) of the two solutions; the fresh RhWT in hydrogen peroxide and the reacted solution under UV exposure. Samples with similar re-emitted radiation signals (voltage) in both the nonirradiated and irradiated (containing potential byproducts) solutions are expected to have the same RhWT concentrations. As these samples also show similar absorbance at 555.5 nm, the presence of potential byproducts are not expected to interfere with RhWT measurements based on its absorbance at 555.5 nm or re-emission at 588 nm.

Results and Discussions

Optical absorbance of rhodamine WT solution

The correlations of the absorbance vs. the concentration of the RhWT solution for hydrogen peroxide concentrations <10 ppm and for three different wavelengths were measured to be:

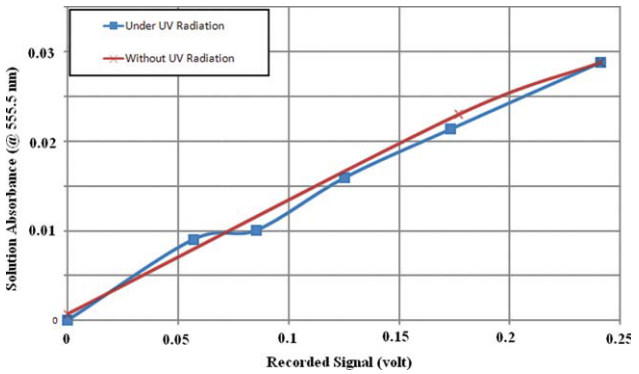

Figure 6. Absorbance of RhWT in hydrogen peroxide solution vs. emitted light captured by photodiode (volt) for different RhWT concentrations.

Cross mark indicates measurement for fresh RhWT under no UV exposures and filled square represents for reactive solution at different exposure UV dose. [Color figure can be viewed in the online issue, which is available at wileyonlinelibrary.com.]

$$\mathrm{ABS}_{532} = \log_{10}\left(\frac{I_{\mathrm{spec}}}{I_{\mathrm{spec},0}}\right) = -(9.85 \pm 0.05) \times 10^{-7} C_{\mathrm{RhWT}} l_{\mathrm{cell}}, \tag{8}$$

$$\mathrm{ABS}_{555.5} = -(2.14 \pm 0.01) \times 10^{-6} C_{\mathrm{RhWT}} l_{\mathrm{cell}}, \tag{9}$$

$$\mathrm{ABS}_{588} = -(1.32 \pm 0.02) \times 10^{-7} C_{\mathrm{RhWT}} l_{\mathrm{cell}}, \tag{10}$$

where ABS, I_{spec}, $I_{\mathrm{spec},0}$, C_{RhWT}, and l_{cell} are absorbance at a specified wavelength, intensity leaving the spectrophotometer cell, intensity entering into the cell, concentration of RhWT solution in ppb, and the light path length of the cell in m, respectively. Consequently, the molar extinction coefficient (ε) of RhWT at wavelengths 532, 555.5, and 588 nm were calculated as 10,900 ± 55, 23,700 ± 111, and 1490 ± 22 m^2/mol, respectively.

Considering the wavelength of the laser source (532 nm), 11% of the laser energy content is absorbed by the medium for a 0.04 m (reactor height) layer of RhWT solution at 126 ppb. This value points to considerable changes in the radiation intensity, which should be taken into consideration by performing separate calibrations for each point in the solution, to find a calibration map (2D) instead of a calibration curve (1D). Using this technique, optical absorbance is integrated into the calibration map with some limitations. The concentration gradient along the laser beam, from top to bottom, should not change significantly (e.g., <35 ppb to achieve an error of <3%). This limitation should be considered in the case of laminar flow, specifically, because no vigorous mixing occurs in the reaction zone in the direction of the laser beam or for high-output UV lamps. In this research, the concentration change over the length of the laser beam did not exceed 35 ppb. If the concentration gradient is high (e.g., at the end of the reactor) or the light pathway is long, the absorbance terms in Equations 2 and 3 should be calculated to reduce the error corresponding to high optical density.

For re-emitted rays at 588 nm from the 126 ppb solution of RhWT, the thickness of the reactor should be controlled (e.g., <8 cm to achieve <3% drops based on absorbance). For this research, the 1 cm thickness of the reactor did not have any significant impact on the absorbance at 588 nm at the maximum concentration.

Direct oxidation of rhodamine WT

The rate of change of the RhWT concentration with an excess of hydrogen peroxide and no UV radiant was calculated to be:

$$\frac{d}{dt}\left(\frac{C_{\mathrm{RhWT}}}{C_{\mathrm{RhWT},0}}\right) = -(8.53 \pm 1.05) \times 10^{-7}, \tag{11}$$

where t and $C_{\mathrm{RhWT},0}$ are time (s) and initial concentration of RhWT, respectively. Based on the rate calculated, after 3.25 h, the concentration of RhWT dropped by only 1%. This means that the direct reaction can be ignored due to the low residence time of the solution inside the reactor (of the order of seconds).

Photolysis of rhodamine WT

RhWT is a persistent chemical under UV exposure; the concentration of RhWT (different solutions from 100 to 800 ppb) did not change after receiving 1000 J/m^2 of UV irradiance. Thus, the photolysis of RhWT can be ignored.

Photo-initiated oxidation of rhodamine WT with hydrogen peroxide and UV radiation

The photo-initiated oxidation rate of RhWT with an excess of hydrogen peroxide after receiving UV irradiance or a UV fluence, H (J/m^2), was calculated to be:

$$\ln\left(\frac{C_{\mathrm{RhWT}}}{C_{\mathrm{RhWT},0}}\right) = (-4.76 \pm 0.09) \times 10^{-3} H \tag{12}$$

The reaction of RhWT with hydroxyl radicals produces other intermediates and by-products. If the concentration of by-products exceeds a certain limit (65% conversion of RhWT), their reactions become dominant, and this correlation would be invalid. As a result, the linear relationship between the received fluence and the log of concentration ratios is only valid for concentrations of reacted RhWT higher than 40 ppb. Equation 12, which considers the overall rate of RhWT degradation by photo-initiated oxidation can be used to calculate the received UV irradiance or fluence at all locations inside the reactor.

Concentration profile in the photoreactor

Figures 7 and 8 show the measured concentration profiles through the reactor in different sections, which are stitched together. Due to the technical limitations, such as difficulties in positioning the cameras at the exact position used for the calibration procedure (±0.005 m), as well as the flow rate fluctuations during the experiments (±0.002 kg/s), the averaged images from the three different sections of the reactor did not overlap perfectly. Also, the values very close to the reactor walls and outlet section of reactor were masked because they did not represent the true concentrations as a

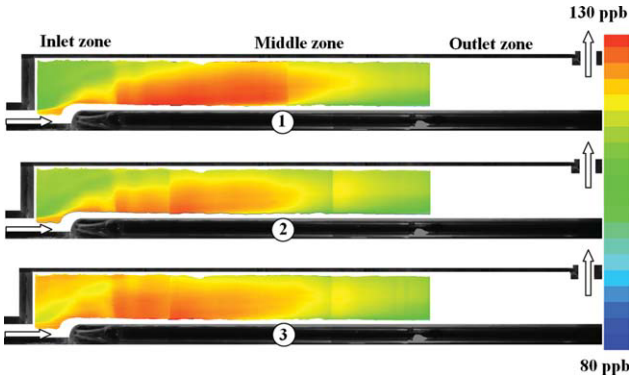

Figure 7. Concentration profile of rhodamine WT (ppb) in the UV reactor at steady-state condition without correction for laser energy variation.

Color bar (linear scale) indicates concentrations from 130 (red) to 80 ppb (blue) and arrows show the flow directions. Illustrations 1–3 are for mass flow rates of 0.006, 0.015, and 0.020 kg/s, respectively. [Color figure can be viewed in the online issue, which is available at wileyonlinelibrary.com.]

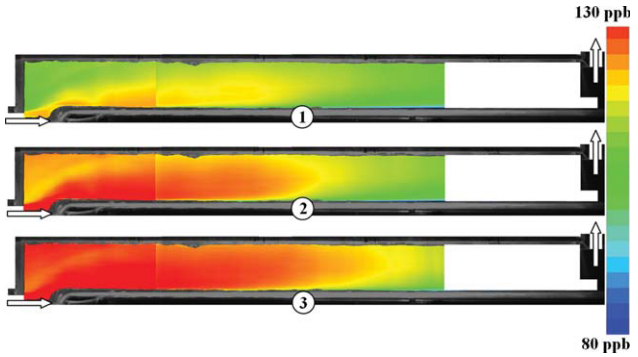

Figure 8. Concentration profile of rhodamine WT (ppb) in the UV reactor with correction for the laser energy variation at steady-state condition.

Color bar (linear scale) indicates concentrations from 130 (red) to 80 ppb (blue), and arrows show the flow directions. Illustrations 1–3 are for mass flow rates of 0.006, 0.015, and 0.020 kg/s, respectively. [Color figure can be viewed in the online issue, which is available at wileyonlinelibrary.com.]

consequence of reflections from the white glue joints in this region of the reactor. For all images, a horizontal median filter with rank 40 was applied to remove the shadowing effects of the laser sheet on the images.

In Figure 7, the concentration is calculated according to the conventional PLIF method without taking into account the laser energy content (i.e., I_0 is omitted). At higher flow rates, higher concentrations of RhWT should extend toward the outlet of reactor; however, this cannot be concluded from the images. This discrepancy was resolved when the laser energy was taken into consideration, as presented in Figure 8.

The "Received Fluence Profile" throughout the reactor is a very useful piece of information. The fluence distribution reveals the local and global performance of a UV reactor, taking all the important phenomena, such as hydrodynamics, UV radiant distribution, and kinetics, into consideration. The fluence profile points directly to the most efficient and deficient zones in the reactor with respect to the reactor performance. The fluence distribution was calculated using Equation 12 for different flow rates in the pilot scale UV reactor as presented in Figure 9.

As shown in Figure 9, at the inlet of the reactor, particularly for Case 1, the received fluence is relatively high. The fluence near the inlet is highest at the lowest flow rate, as can be seen in Case 1 (Figure 9). This is confirmed by considering the profile of concentration in Figure 8, which shows relatively low concentration (e.g., treated flow) at the reactor inlet, particularly at lower flow rates. Mapping the velocity profile in the reactor revealed the reason for the high fluence at the inlet. Particle image velocimetry was applied to measure the velocity profile, using the same system described for the PLIF experiments. Figure 10 shows the measured velocity profile (vector) inside the reactor for a 0.014 ± 0.002 kg/s flow rate.

It is obvious from Figure 10 that part of the flow re-circulates (due to a pressure difference) in the upper part of reactor toward the inlet. This recalculation brings back a portion of the reacted chemicals (bleached) from the middle of the reactor. At lower flow rates (e.g., Case 1), due to the low velocities at the upper left-hand corner of the reactor, the residence time is very high (i.e., the zone is nearly stagnant), and this section receives a higher fluence because of the longer exposure time. At relatively higher flow rates (e.g., Cases 2 and 3), the re-circulating velocities in this section are increased, and the chemicals in this zone are mixed with fresh fluid from the inlet. In the other words, the nearly stagnant zone disappears at higher flow rates causing a more uniform concentration. The back-flow circulation causes the diminishing of the reactant (RhWT) vertical concentration gradient at the entrance of the reactor up to approximately 0.20 m. This effect is more obvious for higher flow rates because of a more vigorous mixing. Once the recirculation effect is reduced at about 0.20 m from reactor inlet, the concentration gradient is more distinguishable with lower

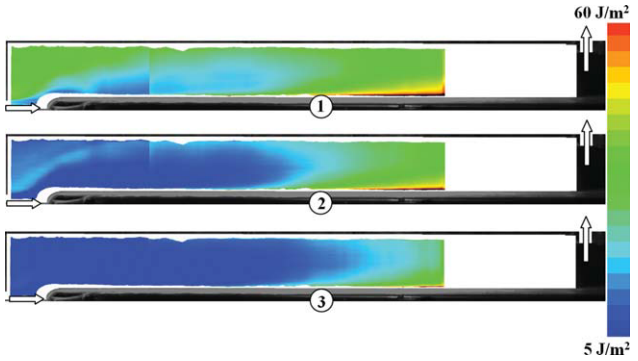

Figure 9. Received UV fluence profile of rhodamine WT (ppb) in the UV reactor under steady-state conditions.

Color bar (linear scale) indicates fluence, from 60 (red) to 5 J/m^2 (blue) and arrows show the flow directions. Illustrations 1–3 are for mass flow rates of 0.006, 0.015, and 0.020 kg/s, respectively. [Color figure can be viewed in the online issue, which is available at wileyonlinelibrary.com].

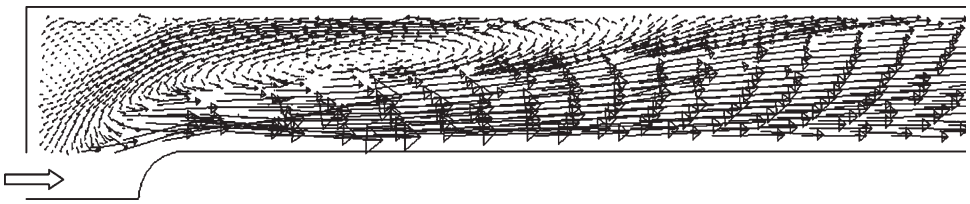

Figure 10. Measured velocity profile inside the reactor using PIV (first half of the reactor).

concentrations closer to the UV lamp, where the photoreaction rate is higher. Figure 9, Case 1 shows a higher receiving fluence at the inlet adjacent to the UV lamp because of a low circulating stream at that location. Figures 9, Cases 2 and 3, clearly shows the mixing effect and residence time of the fresh fluid near the inlet region.

The other important phenomenon is the fluence distribution in the layer close to the lamp. Due to the lack of turbulence in the reactor, turbulent diffusion is omitted, and convective mass transfer dominates, even for higher flow rates. This information is very useful in analyzing the performance of photoreactors and technical optimization.

Source of errors and uncertainties

The procedure presented here for measuring reactive flow using a modified PLIF is a valuable tool for evaluating the performance of UV photoreactors. However, some potential sources of error and uncertainty should be considered when interpreting the data. Some of these are instrumental errors include the ability of a digital camera to effectively capture sequential images, a possible negative effect of temperature on the circuit board of the camera, potential instability of the UV lamp emission (leading to variations in excitation of fluorescent chemical), and imperfect matching of coordinates between the calibration and measured concentration images. Using a digital camera and correcting the coordinates of the images by software considerably reduced these potential sources of errors, but did not eliminate them. Precise quantification of the instrumental errors is impossible. However, the major sources of error and uncertainty are evaluated and addressed below.

The major source of error in the concentration calculation procedure, based on calibration maps, occurs where the concentration gradient is high. These high concentration gradients occur near the ends of the reactor, where the RhWT concentration is very low, close to the UV lamp surface, and high, far from the lamp, due to reaction or recycling of material at the top of the reactor (near the inlet). The maximum error occurs when the concentration at the top is higher (due to a high absorption of light at the reactor exit) than at the bottom. Therefore, all measurements in the outlet sections are expected to have a relatively high degree of uncertainty for all cases (are not shown here). This error could be minimized or eliminated if the equation for the calibration map (Eq. 3) could be derived without the simplifying assumptions concerning the optical density.

The second major source of uncertainty in the calculations is the linear curve fitting for each pixel of the images. Considering uncertainties associated with for each measurement, it can be seen that there is no unique linear function between the captured emitted light (E_c) and the RhWT concentration (C_f). In other words, any of the lines located in a band (between the high and low values of the data considering error bars) could be used in the concentration calculation. The upper and lower bound can be calculated from Equation 3 as:

$$E_c = \left(K_{setup} \pm \Delta K_{setup}\right) I_0 c_f + \left(K_{offset} \pm \Delta K_{offset}\right) \qquad (13)$$

where ΔK_{setup} and ΔK_{offset} are used to calculate the upper/lower values for the slope and intercept. Using Eq. 13, the overall uncertainty (upper/lower value), which contains the effect of all the individual parameters, in the measurement of RhWT concentration was calculated and is shown in Figure 11.

Conclusions

The growing use of UV reactors brings with it the need to improve their performance and develop new measuring techniques for performance evaluation. A modified PLIF method was developed for mapping the concentration and fluence profiles throughout a UV reactor. It was observed that integrating the laser energy into the conventional PLIF and using a 2D calibration map instead of a typical 1D calibration curve increases the accuracy of the measurements.

The method described here provided UV fluence profiles at each cross-section of a photoreactor under various operating conditions and allowed the radial and longitude dispersion of photoreactive chemical to be estimated. The fluence distribution reveals valuable information about the performance of each reactor zone, assisting technical optimization of the reactor.

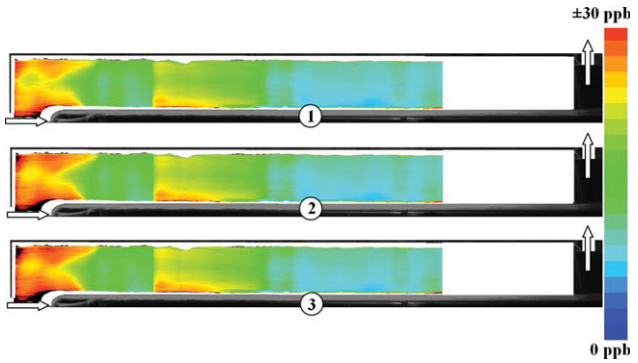

Figure 11. Overall uncertainty in RhWT concentration profile measurement (ppb) with a 95% confidence interval in the UV reactor.

Color bar (linear scale) indicates concentration uncertainty from ±30 (red) to 0 ppb (blue), and arrows show the flow directions. Cases 1–3 are for mass flow rates of 0.006, 0.015, and 0.020 kg/s, respectively. [Color figure can be viewed in the online issue, which is available at wileyonlinelibrary.com.]

Although this technique is a powerful visual diagnostic tool, technical limitations can cause significant errors. As described, if there is a considerable absorption of the laser light or re-emitted light in the system, optical density should be considered in the equations used for calibration and concentration measurements. Most industrial UV reactors operate in the turbulent regime, and the radial concentration gradients are expected to be lower than 500–700 ppb/m, resulting in negligible radiation absorption. Therefore, this method should be applicable without further modification.

Notation

A = area (m^2)
ΔA = active area of the sensor or pixel area on the CCD of a camera (m^2)
ABS_λ = absorbance at wavelength λ
C_{RhWT} = concentration of rhodamine WT (ppb)
$C_{RhWT,0}$ = initial concentration of rhodamine WT (ppb)
c = concentration (mol/m^3)
c_i = concentration of ith component (mol/m^3)
E_c = captured energy (J)
H = local absorbed fluence (dose) by microorganisms or chemicals (J/m^2)
h = Planck's constant (J.s)
I_0 = average radiant intensity of entire spectrum at source of radiation (W/sr)
K_{setup} = setup slope ($sr.s.m^3/mol$)
K_{offset} = setup intercept (J)
l_{cell} = light path length of spectrophotometer cell (m)
$l_{c,p}$ = distance between sensor and emitter (m)
$l_{s,p}$ = distance of investigation point from the light source (m)
P_V = volumetric emitted power (W/m^3)
T_c = fraction of light that reaches the sensor
T_s = fraction of light passing through solution
t = time (s)
ΔV = glowing volume element in the solution (m^3)
x, y, z = Cartesian coordinates (m)
x_c, y_c, z_c = coordinates of the sensor (pixel)
$\varepsilon_{i,\lambda}$ = molar absorption coefficient of spectrum with "λ" wavelength by ith component (m^2/mol)
$\varepsilon_{\lambda e}$ = molar absorption coefficient of solution at wavelength λe nm (m^2/mol)
$\varepsilon_{\lambda s}$ = Molar absorption coefficient of solution at wavelength λs nm (m^2/mol)
Θ_c = quantum efficiency of sensor
Θ_s = quantum efficiency of florescent chemical
θ = angle (radians)
v = frequency (s^{-1})

Literature Cited

1. Kruithof JC, Van Der Leer RC. Practical Eperiences with UV-Disinfection in the Netherlands. Proceedings of the American Water Works Association Seminar on Emerging Technologies in Practice, Annual Conference of the American Water Works Association, Cincinnati, June 17–21, 1990.
2. Office of Water. *Ultraviolet Disinfection Guidance Manual for the Final Long Term 2 Enhanced Surface Water Treatment Rule*. United States Environmental Protection Agency, Washington DC, 2006; EPA 815-R-06-007. Available at: http://www.epa.gov/safewater/disinfection/lt2/pdfs/guide_lt2_uvguidance.pdf.
3. Munter R, Preis S, Kallas J, Trapido M, Veressinina Y. Advanced oxidation processes (AOPs): water treatment technology for the twenty-first century. *Kemia-Kemi*. 2001;28:354–362.
4. Von Gunten U. Ozonation of drinking water: Part I. Oxidation kinetics and product formation. *Water Res*. 2003;37:1443–1467.
5. Kidman RB, Tsuji KS. *Preliminary Costs Comparison of Advanced Oxidation Processes*. Los Alamos National Laboratory, Los Alamos, NM, 1992;LA-12221-MS.
6. Andreozzi R, Caprio V, Insola A, Marotta R. Advanced oxidation processes (AOP) for water purification and recovery. *Catalysis Today*. 1999;53:51–59.
7. Legrini O, Oliveros E, Braun AM. Photochemical processes for water treatment. *Chemical Rev*. 1993;93:671–698.
8. Entrala1 E, Garin YJF, Meneceur P, Hayat M, Scherpereel G, Savin C, Feliers C, Derouin F. Pilot-scale evaluation of UV reactors against in-vitro infectivity of *Cryptosporidium parvum* oocysts. *FEMS Immunol Med Microbiol*. 2007;51:555–561.
9. Cotton C, Passantino L. Regulations in the United States: requirements and guidance for ultraviolet disinfection of drinking water. *J Environ Eng Sci*. 2005;4:S57–S63.
10. Lawryshyn YA, Cairns B. UV Disinfection of water: the need for UV reactor validation. *Water Sci Technol Water Supply*. 2003;3:293–300.
11. Scheible OK, Weber ET. *Verification Test Plan for the Suntec Environmental UV Disinfection for Secondary Effluent Applications Version 3*. US Environmental Protection Agency, Edison, NJ: HydroQual, 2003.
12. Petri B, Cairns W, Gowman L, Mao T. Safeguarding public and environmental health: what are the necessary requirements of UV reactor validation protocols? *J Water Environ Technol*. 2005;3:85–92.
13. Bohrerova Z, Bohrer G, Mohanraj SM, Ducoste J, Linden KG. Experimental measurements of fluence distribution in a UV reactor using fluorescent microspheres. *Environ Sci Technol*. 2005;39:8925–8930.
14. Sen S, Tsai K, Gillis P, Larkins R, Spradling R, Melton LA. Evaluation of Micro-Mixing Models in Simulating Liquid Phase Turbulent Reacting Flow. AIChE Annual Meeting, Dallas, TX, October 31–November 5, 1999, paper 309i.
15. Guilbault GG. *Practical Fluorescence*. New York: Marcel Dekker, 1990.
16. Karasso PS, Mungal MG. PLIF measurement in aqueous flows using the Nd:YAG laser. *Exp Fluid*. 1997;23:382–387.
17. Oppenlander T. *Photochemical Purification of Water and Air*. Wiley-VCH, Weinheim, Germany, 2003.
18. Lipp CW, Gillis PA, Spradling ED, Tsai K, Melton LA. Measurement of Reactive Mixing of Liquids with Combined PIV and Reactive PLIF Methodology. Dow Chemical, Freeport, TX. Available at: http://www.kintecus.com/paper_27_2.pdf, December, 2009.
19. Klassen NV, Marchington D, McGowan CE. H_2O_2 determination by I^{3-} method and by $KMnO_4$ titration. *Anal Chem*. 1994;66:2921–2925.
20. Rahn RO, Stefan MI, Bolton JR, Goren E. Quantum yield of the iodide–iodate chemical actinometer: dependence on wavelength and concentration. *Photochem Photobiol*. 2003;78:146–152.
21. Melton LA, Lipp CW. Criteria for quantitative PLIF experiments using high-power lasers. *Exp Fluid*. 2003;35:310–316.
22. Becker RS. *Theory and Interpretation of Fluorescence and Phosphorescence*, 1st ed. Wiley Interscience, 1969.

Manuscript received Aug. 5, 2009, revision received Dec. 13, 2009, and final revision received Mar. 10, 2010.